MiFuture

Newsletter

MiFuture 2026 Project Review Meeting

Coimbra, 11-13 March

Marie Skłodowska-Curie Actions 30 years Curiosity that changes the world

March 2026

MiFuture Newsletter

Summary

MiFuture held its 2026 Annual Project Review Meeting from 11 to 13 March at the University of Coimbra, gathering all partners and doctoral candidates. The first day focused on reviewing project progress, including research achievements in 6G technologies, and planning upcoming activities across work packages, training, and dissemination. The second day featured a cross-disciplinary entrepreneurship session, combining theoretical insights with group work on innovative business ideas. The event concluded with a joint workshop with the COST 6G-PHYSEC group, including keynote talks on positioning and physical-layer security. Overall, the meeting fostered collaboration, knowledge exchange, and a strong, forward-looking research and training environment.

MiFuture
UMMIMO FOR 6G

MiFuture Newsletter

Day 1 – Project review and work package planning

The MiFuture meeting in Coimbra opened on 11 March 2026 with welcome remarks by Marco Gomes from the University of Coimbra, host and organiser of the event. Ana García Armada, MiFuture Project Coordinator, then welcomed all participants, presented the agenda for the three-day meeting and celebrated the 30th anniversary of the MSCA program. The meeting was held at the Department of Mathematics of the University of Coimbra Representatives of all beneficiaries attended, together with all 15 Doctoral Candidates.

The first session provided an overall review of the project's progress to date. It covered the main management and coordination aspects, including recruitment status, document management, internal procedures, management meetings, deliverables and milestones. The session also highlighted the main research achievements already obtained across the project, such as progress in smart repeaters, cell-free distributed MIMO, OTA and measurement, positioning and channel parameter estimation, OTFS/ISAC signal processing, SLAM and sensing, AI/ML methods for sensing and positioning, and the study of fundamental performance limits.

MiFuture

Newsletter

In addition, the session reviewed the training dimension of the project, confirming that Career Development Plans are already available for all Doctoral Candidates and reporting on the completion of several network-wide and transversal training activities. Feedback collected from the DCs showed a very positive overall assessment of supervision and training quality.

The second session focused on the future activities for WPs 1 to 4. It addressed the next deliverables and milestones planned for 2026 and 2027 and discussed the research objectives to be pursued in the coming phase of the project. The session also examined the balance between academic and industrial periods, the organisation of secondments, and the students' perspective on these experiences, with a view to ensuring that upcoming activities remain well aligned with both the scientific goals of the consortium and the training needs of the Doctoral Candidates. This part of the meeting served mainly to structure the forward planning of the work packages and to prepare the next implementation steps.

The third session was devoted to the upcoming activities for WPs 5 to 7. It reviewed future deliverables for 2026 and 2027, as well as the next planned schools, including activities related to standardisation, 6G vision, and diversity, inclusion and gender issues. The discussion also considered the evaluation of the training programme and the feedback received from the DCs, which pointed to the need for more intensive face-to-face workshops, more hands-on technical content, greater interactivity, and stronger industry-oriented perspectives. In the area of communication, dissemination and exploitation, several concrete proposals were presented, including participation in policy-related events, the preparation of a MiFuture policy brief, the production of audio-visual training materials, the systematic release of data and code repositories, annual press and media actions, outreach activities for European Researchers' Night and Science Week, initiatives to promote STEM studies among women, and participation in technology festivals. Overall, the session helped define a more structured and impact-oriented roadmap for the next phase of the project.

Day 2 – Horizontal Session

On the second day, a cross-disciplinary training session on entrepreneurship took place. The session was delivered by Professors Pedro Sebastião, Rui Ferreira, and Ana Fonseca from Audax ISCTE. Following a theoretical introduction to topics such as technology transfer, development phases, higher education and companies, innovative start-ups and spin-offs, and multidisciplinary knowledge, the students took part in a group workshop in which they were asked to propose an innovative business idea. Each group then presented its proposal, which was discussed and commented on by the lecturers.

MiFuture

Newsletter

The day concluded with an engaging guided tour for the joint MiFuture and COST group around the university and the historic part of the city, followed by a gala dinner at the Hotel Quinta das Lágrimas, where participants also had the opportunity to enjoy an authentic fado performance.

Day 3: Joint MiFuture–COST 6G PHYSEC Technical Session

On the third day, a joint workshop session was held together with the COST 6G-PHYSEC group, bringing together researchers and students around key topics in wireless security, positioning, and future communication systems. The morning opened with two keynote talks: Elena Simona Lohan spoke on Interference Resilience in Satellite-Based Positioning, addressing threats such as spoofing and jamming in GNSS systems, while Stefano Tomasin presented Opportunities and Challenges for Physical Layer Security in Wireless Networks, highlighting the growing importance of physical-layer protection in future wireless standards. This was followed by a special session on physical-layer security for next-generation body area networks, focusing on the ETSI SmartBAN approach.

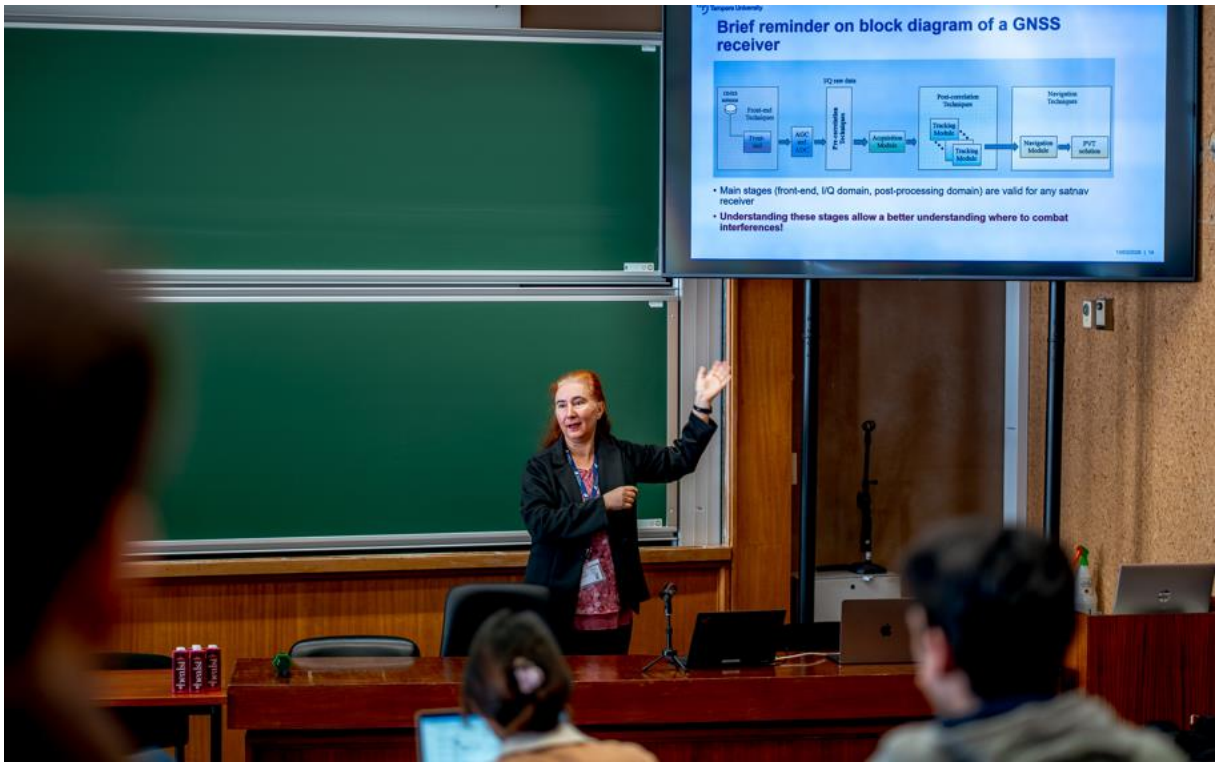

In the afternoon, the students had the opportunity to present their doctoral research projects during a poster session (see the Annex for the posters).

Overall, the meeting proved to be highly productive and enriching for both students and supervisors. It provided a valuable opportunity to meet in person, strengthen connections within the network, exchange ideas, and learn from a wide range of inspiring and forward-looking topics. The combination of academic discussion, interdisciplinary training, and informal interaction created a particularly stimulating environment, reinforcing the collaborative spirit of the project and leaving participants with a strong sense of motivation and optimism for the next stages of their work.

Annex: MiFuture DCs Posters

MiFuture Newsletter

Waveform design for joint communications and sensing

Andrés Reyes Castro*, María Julia Fernández-Getino García*, Carlos Ubeda#
*Department of Signal Theory and Communications, Universidad Carlos III de Madrid, Madrid, España
#Vodafone Intelligent Solutions, Madrid, España

ISAC in 6G

- Integrated Sensing and Communication (ISAC) is a key technology and one of six ITU usage scenarios in 6G networks.
- ISAC requires new waveforms that balance communication reliability and sensing accuracy under challenging conditions, such as high mobility in vehicular and satellite communications.
- ISAC requires the reliable extraction of physical channel parameters, delays and Doppler shifts, directly related to target range and velocity.
- Accurate estimation of these parameters is therefore essential not only for data equalization but also for enabling high-resolution sensing capabilities.

Why OTFS?

Orthogonal Time-Frequency Space (OTFS) operates in the delay-Doppler (DD) domain and provides enhanced robustness to rapid channel variations .

OTFS

OTFS modulates in delay doppler domain.
- High Mobility and Doppler Resilience
- Full Diversity in Delay-Doppler Domain
- Unified waveform for Communication and Sensing
- Robustness to time variant channel

OFDM

Orthogonal Frequency-Division Multiplexing (OFDM) divides the spectrum into multiple orthogonal subcarriers.
- Low Computational Complexity
- Robustness to Multipath and Delay

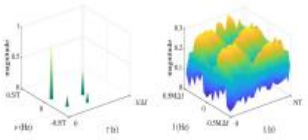

Main challenges

- Fractional Doppler spreads energy across multiple Doppler bins, producing inter-Doppler interference.
- Embedded pilot schemes reduce spectral efficiency due to guard regions.
- High-power pilots for precise channel estimation may increase PAPR, degrading transmitter efficiency.
- Many existing superimposed approaches depend on iterative cancellation and matrix inversions, significantly increasing complexity.

System model

OTFS with Zero-Padding transmitter

We consider a zero-padded OTFS (ZP-OTFS) system operating in the delay–Doppler (DD) domain. Data symbols are first mapped onto an $M \times NM \times N$ DD grid, then transformed to the time domain via the inverse discrete Zak transform (IDZT). Zero padding is appended to prevent inter-block interference. At the receiver, the discrete Zak transform (DZT) maps the received signal back to the DD domain.

Doubly Selective Channel Model [1]

The propagation channel is modeled as:

$$h(\tau,\nu) = \sum_{i=1}^{P} g_i \delta(\tau - \tau_i)\delta(\nu - \nu_i)$$

where:
gi is the complex gain, τi is the delay shift, νi is the Doppler shift.

DD domain Input–Output Model

The equivalent DD-domain received signal is

$$y = Hx + w$$

where:
x is the transmitted DD-domain vector, H is the DD-domain channel matrix, $w \sim CN(0, \sigma_\omega^2)$ is AWGN.

Channel estimation consists of identifying the delay indices, Doppler indices, and complex gains that define H.

Embedded Pilot with Guard Region [2]

Fractional Doppler Channel Estimation

To address fractional Doppler effects, we adopt a single embedded pilot surrounded by full guard regions in the delay–Doppler grid. The guard symbols suppress interference from data, ensuring that the pilot response contains only channel information, especially considering the effect of fractional Doppler.

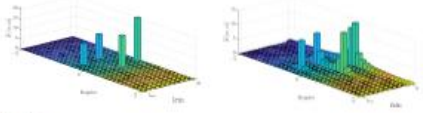

Channel estimation

Channel delays are detected by analyzing the energy variability across Doppler bins.
For each detected delay, the received samples are modeled as a superposition of complex exponentials. We use a Discrete Fourier Transform-based interpolation to refine the Doppler index estimates.
The complex gain is calculated by compensating for Doppler-induced spectral spread and phase rotation.

Superimposed Zadoff–Chu Pilot Scheme [3]

Low-Complexity and Spectrally Efficient Estimation

To improve spectral efficiency and reduce pilot overhead, we propose a superimposed training (ST) strategy based on a delay-wise Zadoff–Chu (ZC) sequence placed in the DD domain. Instead of reserving dedicated pilot resources, the pilot is arithmetically added to the data symbols, preserving all the resources for data transmission.

Constant envelope pilot

A ZC sequence is mapped along the delay axis at the center Doppler bin.
- Constant envelope: no PAPR degradation
- Ideal autocorrelation: strong peak detection
- Robust to noise and interference

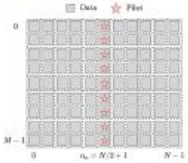

Channel estimation

The DD-domain signal is correlated with the known ZC sequence. Peaks in the correlation map reveal active delay–Doppler pairs and a threshold separates true targets from interference.
Initial channel gains are directly extracted from correlation peaks. If multiple paths share the same Doppler index, a refinement step subtracts overlapping contributions.

Computational Efficiency

The algorithm avoids matrix inversions and iterative detection loops. Its dominant complexity scales as $\mathcal{O}((2k_{max}+1)(2l_{max}+1))$, where k_{max} and l_{max} are the maximum Doppler and maximum delay of the channel, respectively.

Results

Embedded Pilot with Guard Region [2]

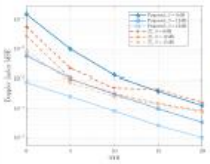

Our proposal lowers Doppler estimation errors, mainly due to the iterative refinement of the Doppler indices.

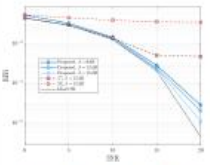

Our proposed method operates close to the ideal CSI scenario and increasing pilot power leads to a slight improvement in BER performance

Superimposed Zadoff–Chu Pilot Scheme [3]

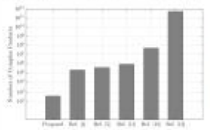

Our proposed method is computationally efficient, eliminating the need for complex iterative techniques.

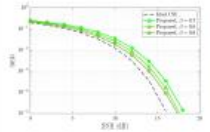

Thee proposed method operates closely to the ideal CSI scenario, confirming its effectiveness.

Main Contributions So Far

- High precision fractional Doppler estimator for OTFS-ISAC.
- Low-complexity superimposed ZC-based channel estimation for OTFS-ISAC.
- Statistical data interference suppression without data-aided cancellation.
- Joint sensing and communication performance validation.

REFERENCES:
[1] Y. Hong, T. Thaj, and E. Viterbo, "Delay-Doppler Communications: Principles and applications," Elsevier, 2022.
[2] A. Reyes-Castro, L. Méndez-Monsanto, K. Chen-Hu, M. J. Fernández-Getino García and A. G. Armada, "Robust Channel Estimation in OTFS Systems Using Embedded Pilots and DFT-Based Interpolation," submitted to the *IEEE 17th International Symposium on Communication Systems, Networks and Digital Signal Processing, CSNDSP 2026*.
[3] L. Méndez-Monsanto, A. Reyes-Castro, K. Chen-Hu, M. J. Fernández-Getino García and A. G. Armada, "OTFS Channel Estimation for ISAC via Superimposed Zadoff-Chu Pilot Sequence," *2025 IEEE International Mediterranean Conference on Communications and Networking (MeditCom)*.

MiFuture
UMMIMO FOR 6G

MiFuture Newsletter

Non-coherent MU-MIMO outperforms MMSE under high-mobility conditions

Rubén de Miguel Gil and Ana García Armada,
Universidad Carlos III de Madrid

Motivation

Ultra-massive MIMO systems based on coherent demodulation face several challenges, specially in high-mobility scenarios:

- Prohibitive reference signal overhead for tracking rapidly time-varying channels.
- Higher numbers of users require higher numbers of pilots.
- High computational complexity required by the best performing coherent schemes (e.g. MMSE).
- Non-coherent schemes mitigate the previous issues but have problems multiplexing high numbers of users.

Non-coherent MIMO

Differential modulation

- Encodes symbols in the differences between transmissions.
- Only needs the channel to be (approximately) constant during two contiguous channel uses.
- No channel estimation is needed.

Coding **Decoding**

$$x_u(n,\nu) = x_u(n,\nu-1)s_u(n,\nu) \longleftrightarrow z_m(n,\nu) = y_m^*(n,\nu-1)y_m(n,\nu)$$

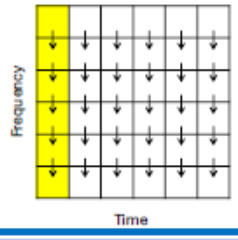

Angular domain processing

The coherence time in the angular domain is larger than in the time domain[1]. Some techniques exploit this:

- **Hybrid processing**: combines coherent equalization with differential coding.
- **Peak selection**: reduces dimensionality and allows the use of more advanced techniques (e.g. BSS).
- **Spatial filtering[2]:** combines legacy non-coherent averaging with a spatial filter.

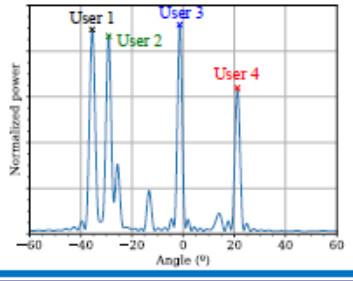

Results

- Ray tracing simulations confirm beam coherence times to be greater than channel coherence times[1].
- Spatial filtering can significantly boost non-coherent MIMO performance[2].
- Good BER scaling with increasing numbers of antennas.
- Angular processing allows for scalable user multiplexing.
- No complex joint constellation design required if the user multiplexing is done in the angular domain.
- Low computational cost due to the lack of matrix inversion operations.
- The higher the mobility, the bigger the performance gap between coherent and non-coherent schemes.

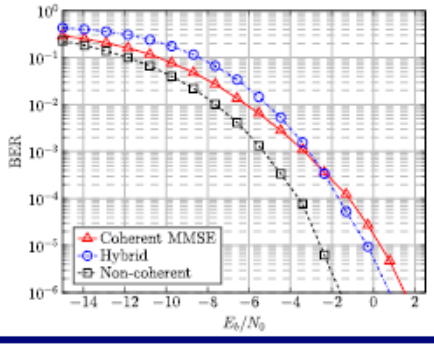

Future Works

- Study solutions for NLOS channels.
- Increase tolerance to spatially correlated channels.
- Testing and implementation (Keysight collaboration).

References

[1] Y. Khorsandmanesh, E. Björnson, J. Jaldén and B. Lindoff, "Beam Coherence Time Analysis for Mobile Wideband mmWave Point-to-Point MIMO Channels," in *IEEE Wireless Communications Letters*, vol. 13, no. 6, pp. 1546-1550, June 2024.

[2] R. de Miguel Gil, K. Chen-Hu, and A. Garcia Armada, "Angle-Domain Multi-User Multiplexing for Non-Coherent Massive MIMO in Rician Channels," 2025 IEEE Global Communications Conference (GLOBECOM), 2025.

Acknowledgements

This project has received funding from the European Union's Horizon Europe research and innovation programme under the Marie Skłodowska-Curie grant agreement No 101119643, ultra-massive MIMO for future cell-free heterogeneous networks (MiFuture).

MiFuture Newsletter

instituto de telecomunicações

DC03 - Positioning Techniques for mmWave D-MIMO Systems

Introduction

Accurate positioning is crucial for 6G applications such as mobility and location-based services. However, in dense urban areas, GPS is often unreliable due to blockage. Millimeter wave (mmWave) distributed MIMO is promising because its wide bandwidth enables high time resolution and accurate time of flight (ToF) ranging. In outdoor urban areas, the downlink signal is frequently non-line-of-sight (NLoS) and affected by multipath reflections. So, each access point (AP) and user equipment can transmit multiple paths with different delays, angles, and received power. If a wrong path is selected, the corresponding range measurement becomes biased. These inconsistent ranges across multiple APs significantly degrade the localization accuracy. This motivates a robust path-selection and range-fusion approach for reliable downlink localization in urban multipath environments.

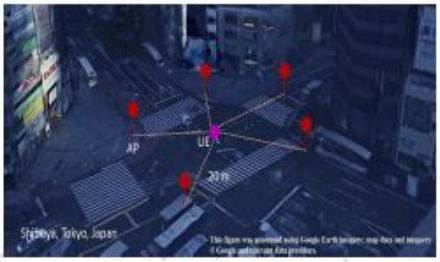

Fig.1: Outdoor Urban Scenario

Scenario and Methodology

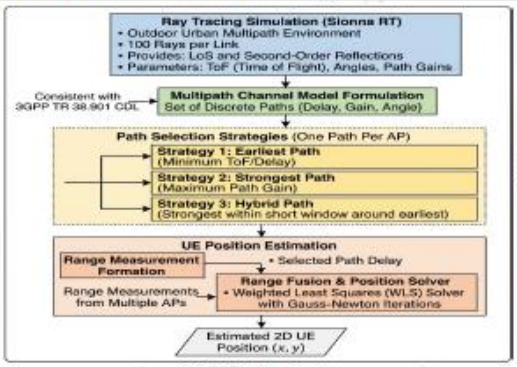

Fig.2: Workflow chart


Fig.3: Ray-Tracing Visualization

Experimental Results

- We consider carrier frequency 28.2 GHz
- 8x8 UPA
- 5 AP and 1 moving UE
- Monte carlo 500
- ToF-based WLS achieves lower localization error than AoA+ToF across all three frames.
- Earliest path selection is more reliable than strongest, since the strongest component can be a reflected path.

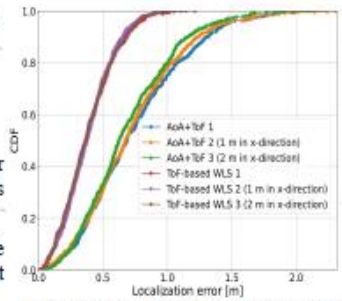

Fig.4: CDF vs Localization error for earliest mode

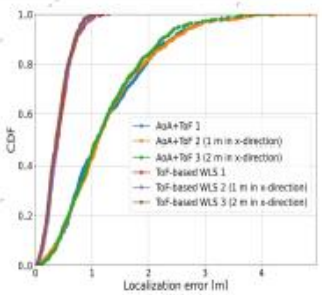

Fig.5: CDF vs Localization error strongest mode

Research Group and Acknowledgements

DC03: Mohd Adnan
Main Supervisor: Professor Adao Silva
Co-supervisor: Professor Rui Dinis
Industrial Supervisor Dr. Lukasz Krzymien

This project has received funding from the European Union's Horizon Europe research and innovation programme under the Marie Sklodowska-Curie grant agreement No 101119643, ultra-massive MIMO for future cell-free heterogeneous networks (MiFuture).

universidad de aveiro

MiFuture Newsletter

MiFuture
UMMIMO FOR 6G

Frequency-Estimation Methods for OTFS Channel Estimation

Omid Abbassi Aghda | o.aghda@campus.fct.unl.pt
Advisors: João Guerreiro, Nuno Souto, Michal Szczachor, Rui Dinis
Instituto de Telecomunicações (IT) & Nokia

Motivation

- Long-distance and high-mobility communications (LDHMC), a key 6G use case, require new modulation schemes.
- OTFS has been introduced to address these challenges
- Accurate channel estimation is essential.
- The channel is modelled in delay-Doppler (DD) domain.
- To acquire the full channel, we need to estimate the delay, Doppler, and gain of each path between the transmitter and the receiver.
- In practice, the true delay and Doppler values do not align with the sampled grid.
- This misalignment introduces fractional delay and fractional Doppler components.
- Existing state-of-the-art channel estimation methods for handling these fractional parameters are highly complex.

Objectives

1. Channel impulse response along Doppler
   - The true channel impulse response exhibits a periodic sinc-like behaviour along the Doppler domain.
   - The channel observed at the receiver is a sampled version of the Doppler-shifted periodic sinc function.
2. Channel impulse response along delay
   - A similar sinc-shaped response appears along the delay axis, with minor approximation differences.
3. Estimation Goal
   - The goal is to estimated the Doppler value k_l out of the sample true channel

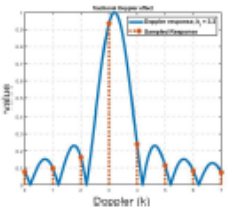

Figure 1. Doppler-domain channel impulse response and the corresponding sampled response seen at the receiver. Doppler shift $k_l = 3.2$

Work Plan

1. Frequency Estimation Problem
   - We observe samples of $s[n] = \sin\left(2\pi n \frac{f}{f_s}\right) + w[n]$
   - The goal is to estimate $f = \frac{k_I + k_F}{N} f_s$, where k_I is the integer part and $k_F \in [-0.5, 0.5]$ is the fractional part.
   - The frequency-domain representation $S[k] = \text{DFT}\{s[n]\}$ exhibits the same periodic sinc-like shape shown in Figure 1.
2. Method to estimate frequency
   - One suitable method is the A&M estimator [1].
   - It first determines the integer component k_I by locating the peak of $S[k]$, and then applies the low-complexity A&M algorithm to obtain the fractional part K_F.
3. Doppler and Delay Estimation in OTFS
   - Since the Doppler and delay estimation problem in OTFS has a similar formulation to the classical frequency estimation problem, the same approach can be extended to estimate OTFS channel parameters.
   - It is important to note that, in OTFS, the estimation must be performed in two dimensions.

Results

1. Complexity

Table 1: Number of complex multiplication for each algorithm

Algorithm	Number of complex multiplications
Proposed A&M LOS	6.512×10^3
Proposed A&M NLOS	3.256×10^4
OCSBI [2]	5.038×10^5
GESBI [3]	2.519×10^5
T-GEESBI [4]	1.167×10^5
GRASBI [5]	1.581×10^5
T-GRAESBI [5]	1.279×10^5

2. Performance

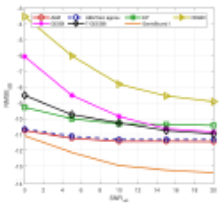

Figure 1. NMSE versus SNR

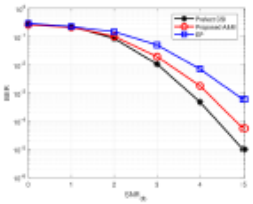

Figure 2. BER versus SNR coded scenario

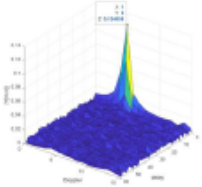

Figure 3. Received DD domain signal implemented using Ettus USRP B210

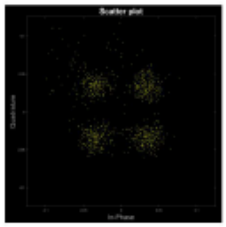

Figure 4. Equalized QAM symbols implemented using Ettus USRP B210.

[1] https://doi.org/10.1109/TSP.2005.843719
[2] https://doi.org/10.1109/TWC.2022.3158616
[3] https://doi.org/10.1109/ICCWorkshops57953.2023.10283794
[4] https://doi.org/10.1109/TWC.2024.3363696
[5] https://doi.org/10.1109/TWC.2025.3532459

* This work was conducted within the MiFuture project, which has received funding from the European Union's Horizon Europe (HE) Marie Skłodowska-Curie Actions MiFuture HORIZON-MSCA2022-ON-01, under Grant Agreement number 101119643 and WAYWAVE HORIZON-MSCA-2022-PF-01, under Grant Agreement number 101108435. The work was partially supported by Portuguese national funds through FCT – Funda„c"ao para a Ci"encia e a Tecnologia, I.P., and, when eligible, co-funded by EU funds under project/support UID/50008/2025 – Instituto de Telecomunica„c"oes, with DOI identifier "https://doi.org/10.54499/UID/50008/2025".

MiFuture Newsletter

Extracting Situational Awareness in 6G Cellular Systems: Robust EKF-SLAM Approach

Ariele Sapienza†, Ossi Kaltiokallio†, Jukka Talvitie†, Fathia Ben Slama‡, Elena Simona Lohan†, Mikko Valkama†
†Tampere University, Tampere, Finland; ‡Allys Technologies, Toulouse, France.

Brief Introduction

Radio-based simultaneous localization and mapping (SLAM) builds upon the SLAM foundations in robotics, where the workhorse algorithm for nearly two decades has relied on an extended Kalman filter (EKF) to jointly estimate the unknown state of the robot and environmental landmarks. However, the EKF-SLAM algorithm has several shortcomings:

1. Quadratic complexity in the number of landmarks [2] making real-time operation challenging for large maps with potentially thousands of landmarks;
2. Very optimistic uncertainty estimates which can cause the EKF filter to diverge [3];
3. High sensitivity to data association (DA) errors which can lead to catastrophic failure of the algorithm [3].

However, the EKF would be an excellent choice for radio SLAM if the DA problem could be solved, because: global maps can be logically divided into submaps using the base station (BS) cells, and secondly, radio SLAM leverages known landmark or anchor locations that provide a preset coordinate system so that filter divergence is not an issue. Thus, **we have tackled the DA problem associated with EKF-SLAM by developing a robust EKF algorithm that can handle severe DA errors making it a very good candidate for radio SLAM.**

Background

We consider a 2D bistatic downlink scenario in which the transmitter (TX) is at the BS side and the receiver (RX) is at the user equipment (UE) side. The location and orientation of the BS is assumed known, whereas the unknown UE state is represented by $\mathbf{x}_k = [x_{\text{UE},k}, y_{\text{UE},k}, \alpha_{\text{UE},k}, b_{\text{UE}}]^T$, that consists of the position $[x_{\text{UE},k}, y_{\text{UE},k}]^T$, heading $\alpha_{\text{UE},k}$ and clock error $b_{\text{UE},k}$ which is used to represent the difference between the unsynchronized BS and UE clocks. The UE then estimates the channel parameters of the stochastic paths. Let $\mathbf{z}_k = [\alpha_1, \phi_1, \alpha_1]^T$ denote the time-of-arrival (ToA), angle-of-departure (AoD) and angle-of-arrival (AoA) estimates of the ith propagation path. Overall, there exist m landmarks in the environment and the joint state of the landmarks forms the map of the environment, denoted by $\mathbf{m} = [\mathbf{m}_1^T, \mathbf{m}_2^T, \ldots, \mathbf{m}_m^T]^T$.

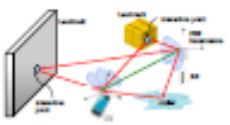

Figure 1: A UE simultaneously localizes itself and builds a map of the environment using downlink positioning reference signal (PRS).

Proposed Robust EKF-SLAM Algorithm

In this paper, we approximate the nonlinear models using local linearization. In addition, the model densities and the joint probability density function (PDF) are approximated using Gaussians such that the online SLAM problem can be solved using the EKF. The approximate joint PDF is given by $p(\mathbf{x}_k, \mathbf{m} \mid \mathbf{z}_{1:k}, \mathbf{s}_{1:k}) \approx \mathcal{N}(\mathbf{x}_k; \hat{\mathbf{x}}_k, \mathbf{P}_k) \mathcal{N}(\mathbf{m}; \hat{\mathbf{m}}_k, \mathbf{P}_{\mathbf{m},k})$, where $\mathbf{z}_{1:k} = [\mathbf{z}_1, \ldots, \mathbf{z}_k]$ denotes the sequence of all observations in which $\mathbf{z}_k = [\mathbf{z}_k^{(1)}, \mathbf{z}_k^{(2)}, \ldots, \mathbf{z}_k^{(n_k)}]$ are the channel parameter estimates of the $n_k + 1$ resolvable paths at time k; $\mathbf{s}_{1:k} = [\mathbf{s}_{1:k-1}, \mathbf{s}_k]$ the sequence of control inputs; and the mean and covariance of the Gaussian approximation are denoted using $\hat{\mathbf{x}}_k$ and $\mathbf{P}_k$, respectively. Update step of the EKF is given by the maximum a posteriori (MAP) estimate which can be viewed as a nonlinear optimization problem.

This work was supported by the MiFuture project under the HORIZON-MSCA-2022-DN-01 call (Grant number: 101119643), by Business Finland under the 6G-ISAC project, and by the Research Council of Finland under Grant number 357730.

Instead of minimizing the negative log posterior which is proportional to the sum of the likelihood and the prior, we propose to minimize:

$$\phi(\mathbf{x}_k) = \frac{1}{2}\|\mathbf{x}_k - \hat{\mathbf{x}}_{k|k-1}\|^2_{\mathbf{P}^{-1}_{k|k-1}} + \frac{1}{2}\sum_{i=1}^{n_k} \rho(\epsilon_k^{(i)}), \tag{1}$$

where $\epsilon_k^{(i)} = \|\mathbf{z}_k^{(i)} - \mathbf{z}(\mathbf{x}_k^{(i)})\|_{\mathbf{R}^{-1}_{k|k-1}}$ is the error and $\rho(\cdot)$ is a robust cost function. There exists many alternatives for selecting $\rho(\cdot)$ including the Cauchy, Huber and Geman-McClure cost functions [4]. In this paper, we choose to use the dynamic covariance scaling (DCS) method since it has a low computational overhead and has shown good performance in graph-based SLAM. The DCS cost function is given by [1, 4]

$$\rho(\epsilon_k^{(i)}) = s_k^{(i)} \epsilon_k^{(i)} + \phi(1 - s_k^{(i)})^2, \tag{2}$$

where $\phi \in [0, 1]$ is a switch variable that controls the influence of measurement ϵ and ϕ is a user defined parameter. Agarwal *et al.* [1] solve for the optimal s_k in closed-form and show that $\rho(\epsilon_k^{(i)}) \leq \epsilon$ holds for every constraint. In theory, s_k can be freely chosen within the interval that satisfies the inequality but the authors propose to use the value that minimizes $\rho(\epsilon_k^{(i)})$ while not exceeding 1, which yields [1]

$$s_k = \begin{cases} 1, & \text{if } \epsilon_k^{(i)} \leq \phi, \\ \frac{2\phi}{\phi + \epsilon_k^{(i)}}, & \text{otherwise.} \end{cases} \tag{3}$$

This constraint makes DCS a quadratic cost function for small errors ($\epsilon_k^{(i)} \leq \phi$), and similar to Geman-McClure for large errors ($\epsilon_k^{(i)} > \phi$). Using DCS, the proposed objective function can now be expressed as

$$\phi(\mathbf{x}_k) = \frac{1}{2}\|\mathbf{x}_k - \hat{\mathbf{x}}_{k|k-1}\|^2_{\mathbf{P}^{-1}_{k|k-1}} + \frac{1}{2}\sum_{i=1}^{n_k} s_k^{(i)} \|\mathbf{z}_k^{(i)} - \mathbf{z}(\mathbf{x}_k^{(i)})\|^2_{\mathbf{R}^{-1}_{k|k-1}}, \tag{4}$$

where $\mathbf{R}_{k|k-1} = \frac{\mathbf{R}_{k|k-1}}{s_k^{(i)}}$ is the scaled measurement covariance. Using DCS, the prediction step of the EKF-SLAM algorithm remains unchanged (see e.g., [2]), whereas the update step of the proposed robust EKF-SLAM algorithm can be computed as:

$$\mathbf{S}_k = \mathbf{C}_k \mathbf{P}_{k|k-1} \mathbf{C}_k^T + \mathbf{R}_k, \tag{5}$$
$$\mathbf{K}_k = \mathbf{P}_{k|k-1} \mathbf{C}_k^T \mathbf{S}_k^{-1}, \tag{6}$$
$$\hat{\mathbf{x}}_{k|k} = \hat{\mathbf{x}}_{k|k-1} + \mathbf{K}_k(\mathbf{z}_k - \mathbf{z}(\hat{\mathbf{x}}_{k|k-1})), \tag{7}$$
$$\mathbf{P}_{k|k} = \mathbf{P}_{k|k-1} - \mathbf{K}_k \mathbf{S}_k \mathbf{K}_k^T \tag{8}$$

Simulation Results

We consider that the DA variable is known and, incorrect DAs are forced with a specified probability and severity to systematically investigate the robustness of the proposed filter to DA errors. We model DA errors using a Gaussian mixture distribution defined as

$$\mathbf{n}_k \sim \sum_{j=1}^{2} w_j \mathcal{N}(0, \Sigma_j), \tag{9}$$

where w_j and Σ_j are the weight and covariance of the jth mixture component. The case $j = 1$ is reserved for the case with no DA error such that: w_1 is the probability of correct DA and $\Sigma_1 = \mathbf{R}_k^2$ is the measurement noise covariance. The case $j = 2$ is reserved for the case when a DA error occurs and the parameters are defined as

$$w_2 = 1 - w_1, \quad \Sigma_2 = (1 + \alpha)\mathbf{R}_k^2 \tag{10}$$

where α controls the severity of the DA error. Setting $\alpha = 0$, the DA error has no impact on the measurement, whereas the impact of the DA error grows as α increases.

The proposed algorithm is benchmarked with respect to the standard EKF-SLAM algorithm and the Rao-Blackwellized particle filter (RBPF)-SLAM algorithm which is implemented using 1000 particles. In addition, we compute the posterior Cramér-Rao bound (PCRB) and the root mean squared error (RMSE) is used as the evaluation metric for the estimators.

As illustrated, the standard EKF is severely impacted by the DA errors even though the number of correct DAs is relatively high ($w_1 = 0.8$). The estimated UE positions and landmarks do not align very well with the ground truth values, especially towards the end of the trajectory. In contrast, the proposed method is robust against DA errors resulting in much better SLAM performance. The estimated UE trajectory closely follows the ground truth trajectory and the estimated landmarks are very close to the true landmarks.

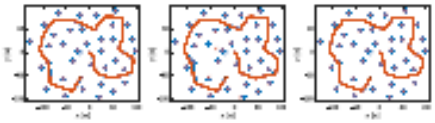

Figure 2: Bistatic radio SLAM illustration for RBPF (left), standard EKF (middle) and the proposed EKF-SLAM algorithm (right). The probability of correct DA is set to 0.8. In each figure, the blue triangle denotes the known BS location. Additionally, solid blue and red lines indicate the true and estimated UE trajectories, respectively, while the blue and red markers denote the true and estimated landmarks.

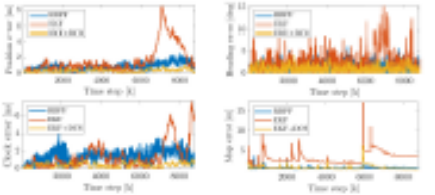

Figure 3: The position, heading, clock and map errors illustrated as a function of time for the different algorithms. The estimated trajectory and map of the algorithms are shown in Figure 2.

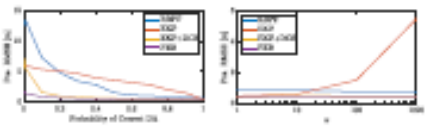

Figure 4: Position RMSEs (averaged over 100 Monte Carlo simulations) and position error bound (PEB) illustrated as a function of probability of correct DA (w_1) on the left and scaling factor (α) on the right. On the left, the scaling factor is fixed to $\alpha = 100$ while on the right, probability of correct DA is set to $w_1 = 0.6$.

References

[1] Pratik Agarwal et al., "Robust map optimization using dynamic covariance scaling", In Proc. 2013 IEEE International Conference on Robotics and Automation (2013), pp. 62–68. DOI: 10.1109/ICRA.2013.6630557.

[2] T. Bailey and H. Durrant-Whyte, "Simultaneous localization and mapping (SLAM): part II", In: IEEE Robotics & Automation Magazine 13.3 (2006), pp. 108–117. DOI: 10.1109/MRA.2006.1678144.

[3] Tim Bailey et al. "Consistency of the EKF-SLAM Algorithm". In: 2006 IEEE/RSJ International Conference on Intelligent Robots and Systems (2006), pp. 3562–3568. DOI: 10.1109/IROS.2006.282326.

[4] Kirk MacTavish and Timothy D. Barfoot. "At all Costs: A Comparison of Robust Cost Functions for Camera Correspondence Outliers". In: Proc. 2015 12th Conference on Computer and Robot Vision (2015), pp. 62–69. DOI: 10.1109/CRV.2015.53.

MiFuture Newsletter

Gaussian Process-Based Extended Object Estimation for 6G ISAC at Millimeter-Wave Frequencies

M. Ertug Pihtili[1] Ossi Kaltiokallio[1] Julia Equi[2] Jukka Talvitie[1] Elena Simona Lohan[1] Ertugrul Basar[1], and Mikko Valkama[1]
[1]Tampere Wireless Research Center, Electrical Engineering Unit, Tampere University, Finland
[2]Ericsson Research, Jorvas, Finland

Motivation & Introduction

6G ISAC (Integrated Sensing and Communication) systems will enable unprecedented environmental awareness by jointly supporting sensing and communication within a single network.

- **Beyond point-scatterer models:** High-resolution mmWave ISAC resolves multiple interaction points (IPs) originating from a single physical object, thereby enabling *extended object* sensing.
- **Extended object:** An object that generates multiple resolvable multipath rays, allowing estimation of its *shape, size, and spatial extent*.
- **Key enablers:** OFDM combined with MIMO at mmWave frequencies provides high resolution in both the delay and angular domains, rendering the IPs of NLoS paths individually distinguishable.
- **Gap in the literature:** Experimental validation of GP-based extended object estimation (EOE) in practical ISAC scenarios remains unexplored.

This work proposes and validates a Gaussian Process (GP)-based EOE method using 5G NR standard-compliant bistatic sensing measurements at 60 GHz and 400 MHz bandwidth, evaluated for both *mapping* and *SLAM* scenarios.

Bistatic Sensing System Model

We consider a bistatic scenario with a known TX location $\mathbf{p}_{\text{TX}}$ and orientation α_{TX}, while the RX state $\mathbf{s}_{\text{RX}} = [\mathbf{p}_{\text{RX}}, \alpha_{\text{RX}}, \delta_{\text{RX}}]^\top$ may be known (mapping) or unknown (SLAM).

The received OFDM signal on the kth subcarrier, lth symbol, mth TX beam, and nth RX beam is:

$$y_{kl}^{m,n} = \sum_{i=0}^{N} \delta_i \, G_{\text{TX}}^{m}(\phi_i) \, G_{\text{RX}}^{n}(\theta_i) \, e^{-j2\pi k \Delta f \tau_i} x_{kl}^{m,n} + w_{kl}^{m,n} \tag{1}$$

Channel parameters $\mathbf{z}_i = [\tau_i, \phi_i, \theta_i]^\top$ (ToA, AoD, AoA) are extracted and used to estimate interaction points (IPs) $\hat{\mathbf{p}}_i$.

GP-Based Extended Object Estimation

Step 1: Clustering IPs with DBSCAN

Estimated IPs are grouped using DBSCAN, yielding clusters $\hat{\mathbf{p}}_i^c$, $i \in \mathcal{I}_c$ per object. Each cluster is converted to polar coordinates centered at the cluster centroid:

$$\begin{bmatrix} \theta_i^c \\ r_i^c \end{bmatrix} = \begin{bmatrix} \text{atan2}(y_i^c - \bar{y}^c, x_i^c - \bar{x}^c) \\ \sqrt{(x_i^c - \bar{x}^c)^2 + (y_i^c - \bar{y}^c)^2} \end{bmatrix}, \tag{2}$$

where $\bar{x}^c = \frac{1}{M_c}\sum_{i\in\mathcal{I}_c} x_i^c$ and $\bar{y}^c = \frac{1}{M_c}\sum_{i\in\mathcal{I}_c} y_i^c$ denote the cluster centers, and $M_c = |\mathcal{I}_c|$ cardinality of the set.

Step 2: GP Regression for Shape Estimation

Each cluster dataset $\mathcal{D}_c = \{[\theta_i^c, r_i^c]^\top\}$ is used to train a GP that maps polar angles to radial distances:

$$r_i = f(\theta_i) + n_i, \quad f(\theta_i) \sim \mathcal{GP}(m(\theta_i), k(\theta_i, \theta_j)) \tag{3}$$

$f(\theta_i)$ is a radial function that maps polar angles to radial distances and is modeled as a GP, enabling shape estimation through the inference of the underlying input–output relationship.

A **periodic squared exponential** (PSE) kernel captures the star-convex shape with 2π periodicity:

$$k(\theta_i, \theta_\ell) = \sigma_f^2 \exp\left(-\frac{2\sin^2\left(\frac{|\theta_i - \theta_\ell|}{2}\right)}{\ell^2} \right) \tag{4}$$

The key predictive equations of the GP, namely the predictive mean and predictive variance, are given respectively as

$$\mathbb{E}[f(\theta_*)] = \mu_* + \mathbf{k}_*^\top (\mathbf{K} + \sigma_n^2 \mathbf{I}_M)^{-1} (\mathbf{r} - \boldsymbol{\mu}), \tag{5}$$

$$\mathbb{V}[f(\theta_*)] = k(\theta_*, \theta_*) - \mathbf{k}_*^\top (\mathbf{K} + \sigma_n^2 \mathbf{I}_M)^{-1} \mathbf{k}_*. \tag{6}$$

In the above, $M = |\mathcal{D}|$ is the number of training points in the cluster, $\mathbf{r} = [r_1, r_2, \ldots, r_M]^\top$, $[\mathbf{K}]_{ij} = k(\theta_i, \theta_j)$, and $\mathbf{k}_*$ is an M-dimensional vector with the ith element being $[\mathbf{k}_*]_i = k(\theta_*, \theta_i)$. The mean of the radial function μ is learned from data such that $\mu_* = \mu$ and $\boldsymbol{\mu} = \mathbf{1}_M \mu$.

Step 3: Hyperparameter Optimization

Hyperparameters $\beta = [\sigma_f^2, \ell^2, \sigma_n^2]^\top$ and mean μ are learned by maximizing the log marginal likelihood:

$$\log p(\mathbf{r} \mid \mu, \beta) = -\tfrac{1}{2}\boldsymbol{\eta}^\top \mathbf{K}_y^{-1} \boldsymbol{\eta} - \tfrac{1}{2}\log|\mathbf{K}_y| - \tfrac{M}{2}\log 2\pi$$

The predictive mean and variance for new test angles θ_* give the estimated object contour and uncertainty.

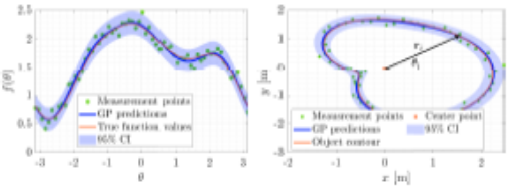

Figure 1. GP-based EOE on synthetic data ($M = 64$ noisy contour measurements). (a) Predicted radial function with 95% confidence interval. (b) Reconstructed star-convex object contour.

Experimental Results: mmWave Measurements

Measurement Setup (Tampere University, Campus Arena):

- TX transmits OFDM PRS; RX collects beamformed signals along a trajectory.
- Both TX and RX equipped with 4 × 16 uniform planar arrays (UPAs).
- Environment: large indoor space with **pillars** (circular cross-section) and **walls**.

DBSCAN yields **7 clusters**: clusters 1, 2, 5, 8 → walls; clusters 3, 4, 6 → pillars.

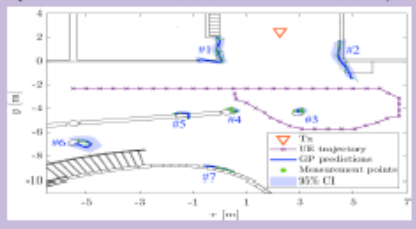

Figure 2. GP-based EOE result for the mmWave *mapping* scenario.

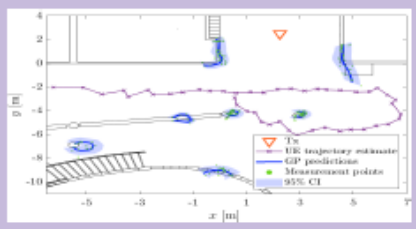

Figure 3. GP-based EOE result for the mmWave *SLAM* scenario.

Key Findings

- **Pillars (circular):** Accurately reconstructed even from partial contours due to smooth radial functions (large ℓ).
- **Walls:** Coarser reconstructions caused by rapidly varying radial functions (small ℓ, e.g., $\ell_{\text{wall}} = 0.23$ vs $\ell_{\text{pillar}} = 1.31$).
- **Mapping vs. SLAM:** Although SLAM IPs are less accurate, the overall EOE performance remains comparable, indicating robustness.
- **Coverage limitation:** A single TX–RX pair observes only partial contours; multiple pairs improve reconstruction.

Conclusion

- Estimates *object shapes*, rather than only point positions, from bistatic NLoS multipath measurements.
- Achieves either fine or coarse shape reconstruction depending on object geometry and the availability of measurements along the object contour.
- Exploits the environmental sensing capability of ISAC systems, where GP-based modeling provides structural insights into extended objects beyond conventional point-scatterer assumptions.
- Enables environmental mapping and identification of static objects with their shapes, which can support improved clutter cancellation and enhance sensing performance.

Funded by EU Horizon Europe MSCA MiFuture (Grant No. 10111964 3).

ertug.pihtili@tuni.fi

MiFuture
UMMIMO FOR 6G

MiFuture Newsletter

Learning-Based User Scheduling for AI-Native Ultra Massive MIMO Systems

Masoumeh Jamshidi | mjamshid@ing.ic3m.es
Supervisor: Professor Ana Garcia Armada | anagar@ing.uc3m.es
University Carlos III of Madrid (UC3M)

Motivation

- Massive MIMO enables simultaneous transmission to multiple users via spatial multiplexing.
- User scheduling is required to select a subset of users in each time slot.
- Optimal scheduling via exhaustive search becomes computationally prohibitive as the number of users increases.
- Greedy algorithms provide practical solutions but still incur significant complexity in large-scale systems.
- Machine learning offers a scalable approach to approximate scheduling decisions with lower computational cost.

Objectives

1. Baseline and Data Generation
   - Implement a greedy user scheduling algorithm as a practical baseline and use its decisions to generate labeled training data for learning.
2. Learning-Based Scheduling
   - Train a supervised machine learning model to approximate the greedy scheduling policy and predict which users should be scheduled based on channel and interference features.
3. Performance and Scalability
   - Evaluate the proposed ML scheduler against the greedy baseline and analyze its scalability compared with computationally expensive approaches such as exhaustive search.

Work Plan

1. Problem Formulation
   - The user scheduling task is formulated as a binary classification problem, where the objective is to determine whether a user should be scheduled for transmission based on its channel and interference characteristics.
2. Learning Strategy
   - A supervised imitation learning framework is adopted. The greedy scheduler serves as a reference policy and generates labeled samples describing the scheduling decisions under varying channel conditions.
3. Model and Scheduling Policy
   - A neural network model is trained to approximate the greedy scheduling policy by learning the mapping between user features and scheduling decisions. During deployment, the trained model assigns a scheduling score to each user, and the users with the highest scores are selected for transmission in each time slot.

PreliminaryResults

1. SINR Performance Comparison
   - The proposed ML-based scheduler is evaluated against the greedy baseline.
   - Simulation results show that the ML scheduler achieves SINR performance close to the greedy algorithm.
   - The ML-based approach significantly reduces computational runtime compared with the greedy scheduler.
   - The learning-based method efficiently scales to scenarios with a large numbers of users.

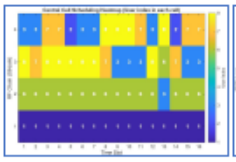

Figure 1: Scheduled Users

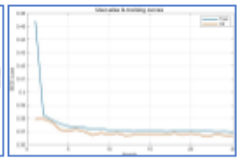

Figure 2: User-wise imitation learning training

1. Training Performance of the ML Scheduler
   - The training curves illustrate the evolution of training and validation loss across epochs during the learning process.
   - The decreasing loss indicates that the neural network successfully learns the greedy scheduling policy.

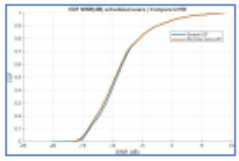

Figure 3: CDF vs. SINR

- This project has received funding from the European Union's Horizon Europe research and innovation programme under the Marie Skłodowska-Curie grant agreement No 101119643, ultra-massive MIMO for future cell-free heterogeneous networks (MiFuture).
- The authors would like to thank Lucia de Miguel Albertos, Carlos Ubeda and Oscar Moreno Vodafone Intelligent Solutions (VOIS) for their valuable feedback and support.

MiFuture Newsletter

Singular value Based Clustering and Access Point selection with Joint Beamforming and Power Optimization in Cell-Free Networks

Prabhat Gupta | prabhat.gupta@co.it.pt
Advisors: Prof. Marco Gomes, Prof. Rui Dinis & Dr. Akshay Jain
Instituto de Telecomunicações (IT) & Nokia Bell Labs Finland

Motivation

6G networks require uniform Quality of Service (QoS), high Spectral Efficiency (SE) and Energy Efficiency (EE) in ultra-dense mobile environments [1]. While Cell-Free Massive MIMO (CF-mMIMO) addresses these needs by using distributed Access Points (APs) to serve users via coherent transmission, it faces major scalability hurdles [2]. As the number of UEs and APs increases, centralized processing becomes computationally complex due to extensive Channel State Information (CSI) acquisition and fronthaul demands [3]. Though current AP selection methods address these issues they rely heavily on Large-Scale Fading (LSF) metrics like pathloss and shadowing [4]. These methods overlook the granular spatial rank structure of multi-antenna channels, which is critical for optimizing performance in multi-stream environments. For the above KPIs to be effective, we need AP selection and resource allocation schemes that jointly exploit the full eigen structure of multi-antenna channels and perform interference aware power control under strict per-AP power and QoS constraints to be energy efficient and providing high QoS at the same time [5].

Objectives

Primary Objective: To maximize the minimum Signal-to-Interference-and-Noise Ratio (SINR) in the network, ensuring fairness among users while strictly enforcing per-AP power constraints and minimum QoS requirements [5].

Innovations:

1. Singular-Value-Based Clustering approach for dynamic AP selection that captures the spatial rank structure of channels, outperforming traditional LSF and graph-based heuristics.
2. To develop a Nested Bisection Algorithm that jointly optimizes power allocation, MMSE beamforming matrices and ensures fairness.

Work Plan

A. System and Channel Modelling:

1. CF-mMIMO downlink model with multiple antenna APs and UEs, NLOS channel with LSF + Rayleigh [7];
2. TDD operation with pilot based MMSE channel estimation with pilot contamination and SE expression with training overhead [2],[3].

B. Singular Value Based Clustering :

1. At each AP, performing local SVD of estimated AP–UE channels and use full singular value matrices as features for k-means clustering;
2. Defining Frobenius-norm distance between singular value matrices, explain elbow-method selection of number of clusters, and the AP–UE assignment to form user-centric clusters;

C. MMSE Beamforming and Joint Optimization:

1. MMSE beamforming formulation and its SVD-based simplification to reduce matrix inversion complexity[2],[7];
2. Formulating the max–min SINR optimization problem with per-AP power and per-UE QoS constraint, highlighting non-convex coupling of beamformers and power;
3. The nested bisection algorithm where outer bisection is on target SINR and inner bisection on power vector with iterative MMSE beamformer updates and per-AP power scaling [5].

Preliminary Results

1. Spectral Efficiency (SE) and Fairness:
   - The proposed *Clustering + Bisection* method achieves an approximate 7.7x improvement in median minimum SE.
   - The method successfully equalizes SINR, achieving the highest Jain's Fairness Index (JFI) of 0.80 [8].
   - The Probability Density Function (PDF) shows a sharp concentration of user rates between 2.0–2.5 bits/s/Hz, confirming that the majority of users meet the target QoS.
2. Energy Efficiency (EE) and Power Optimization
   - It yields a 2.67x improvement in EE (112.44 Mbits/Joule) compared to LSF-based methods (42.66 Mbits/Joule) [9].
   - AP selection using clustering minimizes spatial leakage and reduces the computational load on the CPU.
   - Bisection algorithm dynamically lowers power to reduce interference, enhancing system scalability.
3. Pilot Contamination
   - Under pilot contamination ($\tau_p = 15$) while median performance drops by ~67%, the optimized framework still maintains higher fairness than unoptimized heuristics [11].

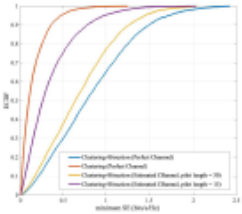

Figure 1. CDF of minimum SE

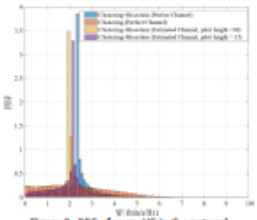

Figure 2. PDF of every UE in the network

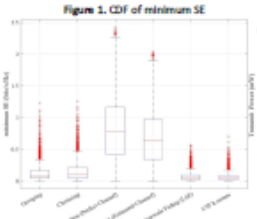

Figure 3. Minimum SE across different methods.

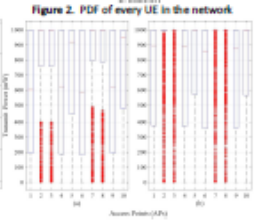

Figure 4. Transmitted Power from the APs for clustering+bisection. (a) τ_p= 30 (b) τ_p = 15

References: References are available at this QR code

* This project has received funding from the European Union's Horizon Europe research and innovation programme under the Marie Skłodowska-Curie grant agreement No 101119643, ultra-massive MIMO for future cell-free heterogeneous networks (MiFuture).

MiFuture Newsletter

Collaborative Radio SLAM

Radovan Juran [1,2] Ossi Kaltiokallio [2] Julia Equi [3] Jukka Talvitie [2] Elena Simona Lohan [2] Mikko Valkama [2]

[1]Tampere Wireless Research Center, Electrical Engineering Unit, Tampere University, Tampere, Finland
[2]Department of Telecommunications, Brno University of Technology, Brno, Czech Republic
[3]Ericsson Research, Jorvas, Finland

Bridging Communication and Sensing

Integrated Sensing and Communication (ISAC) is a key paradigm of the 6G networks concept [1], transforming the conventional connectivity-driven radio interface into a joint *communication-sensing platform* with situational awareness capabilities.

Environmental sensing is fundamental in vehicular applications, enhancing location awareness and localization performance [2], making the ISAC-based SLAM one of the promising, yet challenging directions towards context awareness and safety [3].

Motivation

Positioning and tracking of non-connected objects for vehicular safety with millimeter wave frequencies

Future connected vehicles require precise situational awareness [1, 2, 4].

Urban traffic densities can reach up to 12,000 vehicles/km² [5], with representative heavy urban scenarios around 2,000 vehicles/km² [5]. Such environments consist of heterogeneous traffic (connected and unconnected vehicles) [6, 7].

As the proportion of connected vehicles increases, dense traffic becomes a natural enabler of collaborative radio SLAM (Figure 1):

- more cooperating UEs → larger jointly explored area,
- shared observations → richer sensing,
- increased information → reduced estimation uncertainty.

This creates opportunity for a scalable collaborative localization and mapping.

Improving Radio SLAM via Information Sharing

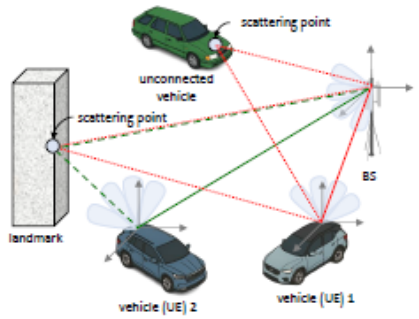

Figure 1. Vehicular collaborative radio SLAM use case bridging communication and sensing. Vehicles exploit multipath reflections from infrastructure and surrounding traffic participants to achieve cooperative positioning and environment mapping beyond line-of-sight conditions.

What are the fundamental performance limits of collaborative SLAM?

Simulation Environment

Figure 2 shows the 200×200 m map with a BS (TX) at known location and N static landmarks. The M UEs (RX) follow a road-like trajectory defined by 17 reference waypoints, with each UE traversing a randomized variant to emulate realistic lane-level deviations. Bistatic downlink setup is considered with LoS signals always available and single-bounce NLoS measurements from landmarks within a 50 m radius.

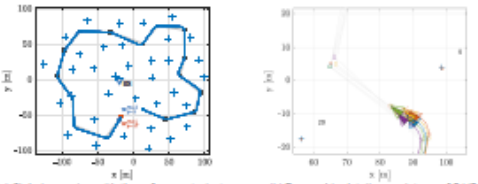

(a) Global map view with the reference trajectory (b) Zoomed-in detail on a platoon of 5 UEs

Figure 2. The map shows the base station (BS) as a blue triangle (▽), the N landmarks as crosses (+), and the path waypoints as squares (□), traversed by the UEs starting from $\mathbf{w}_1^1$ (■) to $\mathbf{w}_{11}^1$ (■) by default.

For benchmarking, the bounds derived consider a centralized processing approach based on EKF SLAM, where all the information is available in one place, to provide an analytical method for system design and pre-deployment performance evaluation.

Fundamental Accuracy: Posterior Cramér–Rao Bounds

The Posterior Cramér-Rao Bounds (PCRB)

The best achievable estimation accuracy given system dynamics and measurements, assuming:

$$\mathbf{P}_k \geq \mathbf{J}_k^{-1} \tag{1}$$

where $\mathbf{J}_k$ is the posterior Fisher Information Matrix (FIM). Employing the recursive formulation of the posterior FIM [8], the bound evolve as:

$$\mathbf{J}_k = \underbrace{(\mathbf{F}_k \mathbf{J}_{k-1}^{-1} \mathbf{F}_k^\top + \mathbf{Q}_k)^{-1}}_{\mathbf{J}_{\text{prior}}} + \underbrace{\mathbf{H}_k^\top \mathbf{R}_k^{-1} \mathbf{H}_k}_{\mathbf{J}_{\text{data}}}, \tag{2}$$

where $\mathbf{F}_k$ is dynamics Jacobian, $\mathbf{Q}_k$ process noise, $\mathbf{H}_k$ measurement Jacobian, $\mathbf{R}_k$ measurement noise, and $\mathbf{J}_k$ the posterior FIM.

Evaluating the Achievable Performance

At each time step k, the limits are extractable from FIM for position error bound (PEB), heading error bound (HEB), clock error bound (CEB) and landmark error bound (LEB) for the mth of the M user equipments (UEs) and nth landmark as:

$$\text{PEB}_k^{(m)} = \sqrt{([\mathbf{J}_k^{-1}]_{i,i} + [\mathbf{J}_k^{-1}]_{i+1,i+1})}, \tag{3}$$

$$\text{HEB}_k^{(m)} = \sqrt{([\mathbf{J}_k^{-1}]_{i+2,i+2})}, \tag{4}$$

$$\text{CEB}_k^{(m)} = \sqrt{([\mathbf{J}_k^{-1}]_{i+3,i+3})}, \tag{5}$$

$$\text{LEB}_k^{(m)} = \sqrt{([\mathbf{J}_k^{-1}]_{j,j} + [\mathbf{J}_k^{-1}]_{j+1,j+1})}, \tag{6}$$

in which $i = 4(m-1)$ and $j = 4M + 2(n-1)$.

References

[1] N. González-Prelcic, M. Furkan Keskin, O. Kaltiokallio, M. Valkama, D. Dardari, X. Shen, Y. Shen, M. Bayraktar, and H. Wymeersch, "The Integrated Sensing and Communication Revolution for 6G: Vision, Techniques, and Applications," *Proceedings of the IEEE*, vol. 112, no. 7, pp. 676-723, Jul. 2024.

[2] A. Behravan, V. Yajnanarayana, M. F. Keskin, H. Chen, D. Shrestha, T. E. Abrudan, T. Svensson, K. Schindhelm, A. Wolfgang, S. Lindberg, and H. Wymeersch, "Positioning and sensing in 6G: Gaps, challenges, and opportunities," *IEEE Vehicular Technology Magazine*, vol. 18, no. 1, pp. 40-48, 2023.

[3] H. Wymeersch, N. Garcia, H. Kim, G. Seco-Granados, S. Kim, F. Wen, and M. Pratte, "5G mm-Wave Downlink Vehicular Positioning," in *Proc. IEEE GLOBECOM 2018*, Abu Dhabi, United Arab Emirates, Dec. 2018, pp. 206-212.

[4] Y. Ge, O. Kaltiokallio, F. Rastegarnia Roj, M. F. Keskin, H. Chen, D. Jones[...], Talvitie, M. Valkama, F. Hofmann, and H. Wymeersch, "Sensing with mobile devices through radio SLAM: Models, methods, opportunities, and challenges," *IEEE Communications Magazine*, vol. 63, no. 12, pp. 80-87, 2025.

[5] NGMA, "C-V2X use cases and service level requirements, volume II," 5G Automotive Association (5GAA), Technical Report, Jan. 2020.

[6] X. Zhang, J. Li, J. Zhou, S. Zhang, J. Wang, S. Yuan, [...] Liu, and Q. Li, "Vehicle-to-Everything Communication in Intelligent Connected Vehicles: A Survey and Taxonomy," *Automotive Innovation*, vol. 8, no. 1, pp. 73-85, Feb. 2025.

[7] Z. Cheng, J. Zhu, Z. Feng, W. Yang, W. Zhang, and J. Chen, "Driving Safety Risk Analysis and Assessment in a Mixed Driving Environment of Connected and Non-Connected Vehicles: A Systematic Survey," *IEEE Transactions on Intelligent Transportation Systems*, vol. 26, no. 5, pp. 5747-5767, May 2025.

[8] P. Tichavsky, "Posterior Cramer-Rao bound for adaptive harmonic retrieval," *IEEE Transactions on Signal Processing*, vol. 43, no. 5, pp. 1299-1302, May 1995.

The Benefits of Collaboration

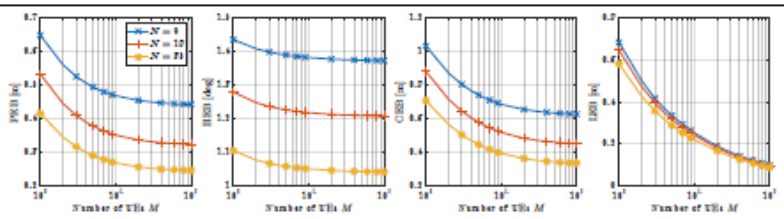

Figure 3. The PCRB lower bounds on estimation accuracy averaged over 100 Monte Carlo simulations per each M of UEs at different landmark density N.

MiFuture Newsletter

MiFuture
UMMIMO FOR 6G

KU LEUVEN
KEYSIGHT

End-to-End Experimental Validation
of RIS and Passive Reflectors in mmWave 5G Systems

João Ferreira[1,2], Ansgar Leßmann[1], Carles Navarro Manchón,[1], Dominique Schreurs[2]
[1]*Keysight Technologies*
[2]*KU Leuven*

MiFuture

Introduction

Millimeter-wave (mmWave) 5G links offer large bandwidth but suffer from severe path loss and frequent blockage, leading to coverage gaps in non-line-of-sight conditions. Reconfigurable Intelligent Surfaces (RIS) and passive reflectors (PR) can redirect energy to restore connectivity. In this work, we connect laboratory characterization to live-network field trials by performing an assessment of RIS and PR performance in a controlled environment. Scattering, link quality and sensitivity analysis and conducting field trials considering challenging NLoS for RIS and PR.

Measurement setup and KPIs

Controlled characterization: RIS and passive reflectors (PR) are measured in a modified compact antenna test range (CATR, IFF-NF) anechoic chamber, enabling repeatable **angle sweeps** and **wideband captures** with controlled polarization and geometry.

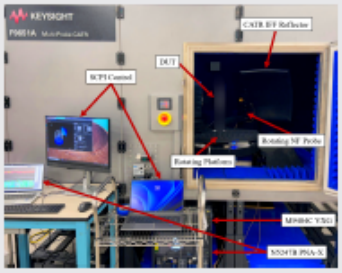

HPBW: $\mathrm{HPBW}(f) = \theta^{+}_{-3\mathrm{dB}}(f) - \theta^{-}_{-3\mathrm{dB}}(f)$

Pointing error: $\Delta\theta(f) = \theta_{\mathrm{peak}}(f) - \theta_{\mathrm{target}}$

Spec. Supression: $\mathrm{SSR}(f) = 10\log_{10}\left(\frac{P_{\mathrm{main}}(f)}{P_{\mathrm{spec}}(f)}\right)$

3-dB bandwidth: $\mathrm{BW}_{3\mathrm{dB}} = f_2 - f_1$

EVM: $\mathrm{EVM}_{\mathrm{RMS}} = \sqrt{\frac{\sum_{n=1}^{N}|s_n - \hat{s}_n|^2}{\sum_{n=1}^{N}|s_n|^2}}$

ACPR: $\mathrm{ACPR} = 10\log_{10}\left(\frac{P_{\mathrm{adj}}}{P_{\mathrm{main}}}\right)$

Field Trials setup

Scenario A

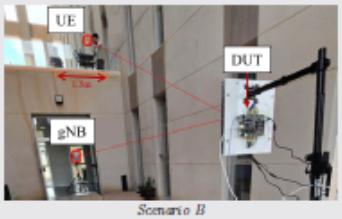

Scenario B

Acknowledgements

This project has received funding from the European Union's Horizon Europe research and innovation programme under the Marie Skłodowska-Curie grant agreement No 101119643, ultra-massive MIMO for future cell-free heterogeneous networks (MiFuture).

Scattering behaviour

The assisted mmWave link is governed by the surface **angle-frequency scattering response**: changes in angle/frequency shift the **main lobe** and **specular leakage**, directly affecting **gain/SNR** and thus **EVM/ACLR**.

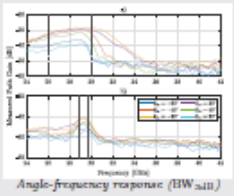

Angle-frequency response ($\mathrm{BW}_{3\mathrm{dB}}$)

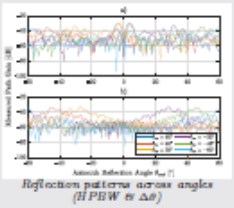

Reflection patterns across angles (HPBW & $\Delta\theta$)

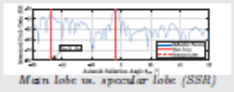

Main lobe vs. specular lobe (SSR)

Signal Quality and Non-Linear behaviour

DUT	θ_{out}	θ_{in}	C. Gain	EVM	ACPL	ACPU
RIS A	30°	0°	-34.81	0.45	-43.75	-43.15
	45°	0°	-46.64	2.69	-32.09	-31.41
RIS B	30°	0°	-48.73	3.72	-36.05	-34.72
	45°	0°	-48.88	4.08	-30.27	-29.03
RIS C	30°	0°	-51.65	5.70	-26.74	-26.23
	45°	0°	-52.48	5.80	-26.10	-25.42

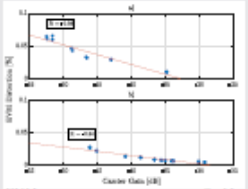

EVM versus carrier gain (1024-QAM).

EVM follows carrier gain (SNR-limited trend), suggesting that the dominant impairment is the link budget rather than device-induced **nonlinear distortion**. This also explains why small pointing errors (reducing gain by a few dB) translate into visible EVM degradation.

Sensitivity analysis and field-trial results

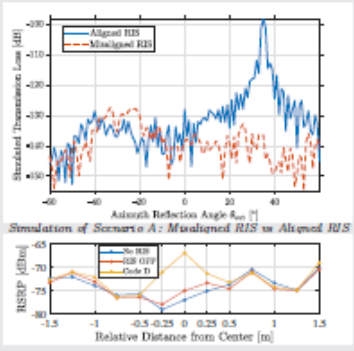

Simulation of Scenario A: Misaligned RIS vs Aligned RIS

Field trial in Scenario B: representative NLoS configuration for validation.

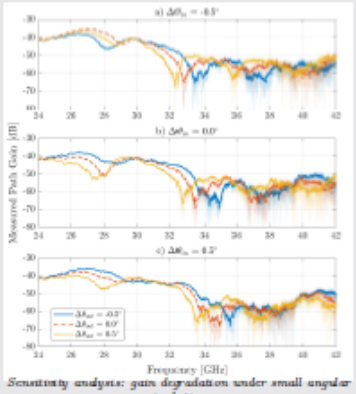

Sensitivity analysis: gain degradation under small angular perturbations.

Both RIS and passive reflectors are **highly sensitive to sub-degree misalignment**. Scenario A (longer distances, tighter angular tolerance) loses the assisted path under **open-loop pointing errors**, while Scenario B (shorter range, favorable geometry) provides **enough alignment margin** to observe a repeatable RIS impact.

Conclusion

This work provides an end-to-end experimental validation of RIS and passive reflectors for mmWave 5G, linking controlled chamber characterization to wideband signal-quality measurements and field-trial observations.

MiFuture
UMMIMO FOR 6G

MiFuture
Newsletter

Partial Relaxation for Near-Field Channel Parameter Estimation: Algorithms and Cramer–Rao Bounds

SPCOMNAV UAB Universitat Autònoma de Barcelona

Mohammad Abu Aqoulah[1,2], Gabor Fodor[2], Gonzalo Seco-Granados[1]

SPCOMNAV research group, School of Engineering, Universitat Autònoma de Barcelona (UAB) [1]
Ericsson Research, Stockholm, Sweden [2]

Problem statement

- Large antenna arrays in 5G/6G systems may place users in the **radiative near-field region**, where the conventional far-field plane-wave assumption no longer holds.

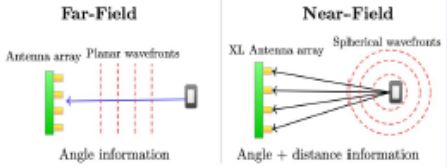

System Model

We consider a multiuser uplink scenario where a base station employs an **N-element Uniform Linear Array (ULA)** and collects **L snapshots** from **K users** located in the **radiative near-field region**. Each user k is described by a **distance–angle pair (d_k, ϕ_k)** measured with respect to the array reference point.

Received signal model (ℓ-th snapshot):

$$\boldsymbol{y}[\ell] = \sqrt{P_s}\boldsymbol{H}\boldsymbol{D}_{\boldsymbol{\psi}}\boldsymbol{s}[\ell] + \boldsymbol{w}[\ell],$$

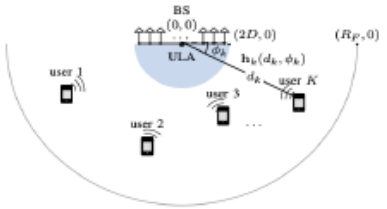

H : near-field multiuser channel matrix.
s[ℓ] : transmitted symbol vector.
Dψ : diagonal matrix of per-user phase offsets.
w[ℓ] : additive complex Gaussian noise.
$\mathbf{P_s}$: transmit symbol power.

Users lie in the radiative near-field, i.e., at distances between 2D (twice the array aperture) and the Fraunhofer range R_F.

Proposed Methods and Performance Bounds

PR-based Algorithms

- **PR-ML:** assumes known pilot symbols and estimates the user parameters via likelihood maximization after interference projection.
- **PR-CF:** operates without pilots and estimates parameters using covariance fitting.

Performance Bounds

- **PR-CRB$_\psi$ / PR-CRB$_s$:** Cramér–Rao bounds derived under the **Partial Relaxation** framework for the known-pilot and unknown-symbol cases.

Partial Relaxation Concept

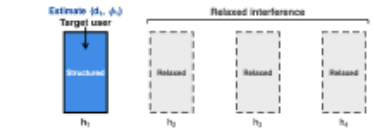

Estimate the target user parameters while modeling the other users as unstructured interference

Experimental Results

- Performance is evaluated in terms of **NMSE** for near-field multiuser channel estimation.
- As a baseline, we consider **2D-MUSIC** (Two-Dimensional Multiple Signal Classification).
- The proposed **PR-ML** and **PR-CF** are compared with 2D-MUSIC and their corresponding CRB bounds.
- **PR methods outperform 2D-MUSIC** across the SNR range and approach their bounds with fewer snapshots.

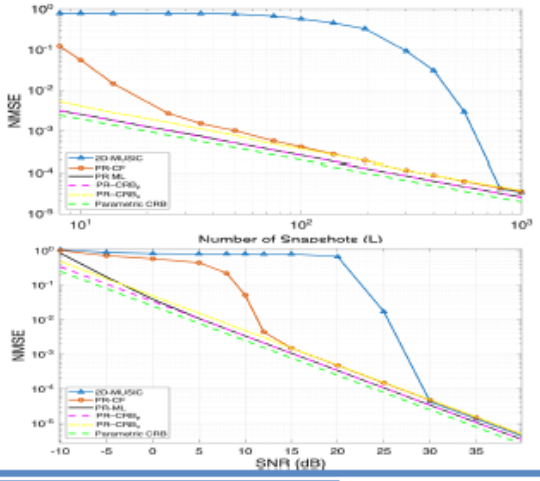

Conclusions

- Proposed a **Partial Relaxation framework** for multiuser **near-field parameter** estimation.
- Developed **PR-ML** and **PR-CF** estimators with corresponding CRB bounds.
- The proposed methods **outperform 2D-MUSIC** and approach their bounds at practical SNR and snapshot levels; **future work** will extend the framework to incorporate NLoS components.

References

[1] M. Abu Aqoulah, D. Gürgünoğlu, G. Fodor, and G. Seco-Granados, "Partial Relaxation for Near-Field Channel Parameter Estimation: Algorithms and Cramér–Rao Bounds," **accepted for presentation** at IEEE International Conference on Communications (ICC), 2026.

Acknowledgement

This project has received funding from the European Union's Horizon Europe research and innovation programme under the Marie Skłodowska-Curie grant agreement No 101119643, ultra-massive MIMO for future cell-free heterogeneous networks (MiFuture).

MiFuture
UMMIMO FOR 6G

MiFuture Newsletter

LUND UNIVERSITY

A measurement-based analysis of repeater assisted cellular massive MIMO channels

ALEKSANDAR BIRMANCEVIC*, YINGJIE XU*, SARA WILLHAMMAR*, FREDRIK TUFVESSON*
*DEPARTMENT OF ELECTRICAL AND INFORMATION TECHNOLOGY, LUND UNIVERSITY

Abstract

Repeater-assisted cellular massive multiple-input multiple-output (MIMO) has recently gained attention by showing the potential to improve the performance of cellular massive MIMO, approaching that of distributed MIMO.
A measurement campaign has been carried out in an indoor environment with a co-located massive MIMO array, and for different scenarios with four single-antenna users in either line-of sight (LoS) or non-LoS (NLoS), and for various multi-antenna repeater deployments.
We analyze and compare the channel characteristics and power distributions, with and without repeaters, providing insights into real channels for repeated-assisted cellular massive MIMO systems.

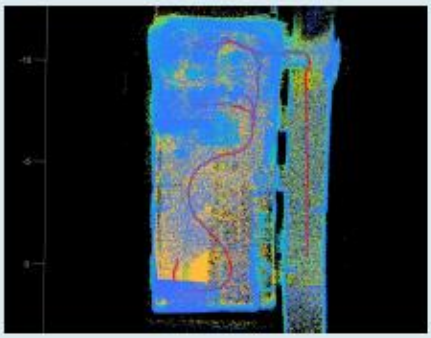

Measurement Campaign

A mobile robot with 4 antennas represents a group of closely-spaced UEs. The UE antennas were configured with various orientations to capture polarization diversity. The robot traversed the room, exhibiting dynamic LoS and NLoS propagation to the BS and repeaters.

- Carrier frequency: 5.67 GHz
- Bandwidth: 400 MHz
- Number of UE antennas: 4 (single monopole antenna)
- Number of repeater antennas: 64 (16 antenna ports, 4 panels)
- Number of base station antennas: 64 (16 antenna ports × 4 panels)

Performance Evaluation

- The measured absolute channel gain of the top left UE to the BS in duration of 10 seconds was analyzed.
- The UE – BS link without the contribution of RPs (upper figure) and part of the repeater's link (RP's antenna port to BS, lower figure) in NLoS conditions are given.

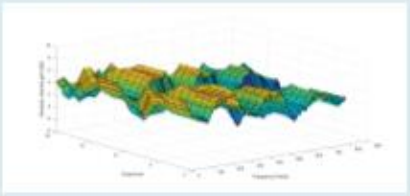

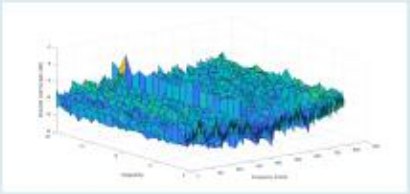

Conclusion

The needs for the coverage improvements and capacity increase in the indoor scenario was identified. The measurement data aim to show how does the positions and orientation of UEs affects the channel gains with and without repeaters involved.

Contact

Aleksandar Birmancevic
Lund University, Sweden
aleksandar.birmancevic@eit.lth.se

MiFuture
UMMIMO FOR 6G

MiFuture Newsletter

Machine Learning-based Environment Awareness for Enhanced Communication and Sensing

LUND UNIVERSITY

PAUL BERESTESKY, OVE EDFORS (Academic Supervisor)
Department of Electrical and Information Technology, LTH, Lund University, Lund, Sweden

Objective

To address **environmental awareness** using **machine learning** (ML) in an approach based on a combination of offline prior knowledge, e.g., **model-based ray tracing**, and information gathered during operation, e.g., measurements between base stations (BS) and user equipment (UE).

Map data will be used to produce an initial model of the local environment, which may be further refined using measurements collected as part of an initialization procedure. Adjustment of the model will continue using operational traffic between BSs and UEs. ML methods will be employed in implementation of the model, which can be used to more effectively direct **communication and sensing** actions within the network.

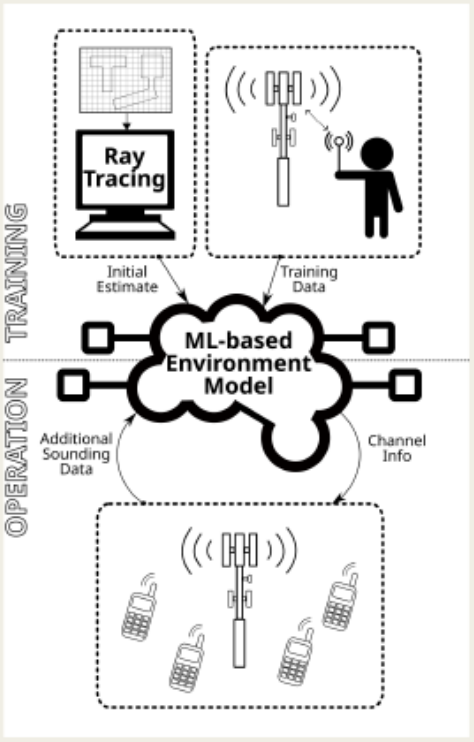

Benefits of Approach

- Availability of prior environmental knowledge reduces or eliminates the need for determination of channel state for each new connection and frees timeline from channel sounding actions. The cost from such actions in an **UmMIMO** system with large dimensions becomes significant and burdensome.
- More effective than using simple geometric assumptions, e.g., direct pointing of beam based on endpoint location vs accounting for occlusions or alternate non-direct paths.
- Achieve what cannot be achieved with training alone, e.g., dealing with non-cooperative nodes such as malicious eavesdroppers or mapping reception "dead zones."

Challenges

The environment model must contain channel information in some useful form ranging from codebook index to full list of weights across all antenna elements. It must hold information for a set of coordinates across the 2D or 3D space that it covers with adequate resolution and may allow for look-up based on UE position alone for BS-to-UE links or on two arbitrary positions if UE-to-UE links are to be supported. This translates to a very large amount of information and strongly motivates the use of ML to implement the environment model.

Project Methodology

- Develop and test algorithms using environmental data sets from a range of sources:
  - Low fidelity, simulation outputs: Finite-Difference Time-Domain for truth, ray tracing for environment model initialization source. Generated at will. Allows for full control of initial learning studies.
  - Medium fidelity, real measurement sets: real data collected in simple small-scale scenarios, limited number of antenna elements, moderate volume coverage. Relatively low-effort data collections.
  - Higher fidelity, real measurement sets: real data collected in more elaborate large-scale scenarios, greater number of antenna elements, large volume coverage.
- Investigate variations in multiple aspects of the problem, for example
  - ML approaches and architectures
  - Channel information types, e.g., beam direction vs full set of antenna element weights
  - Practical details, e.g., training in operation

References

Y. Zeng *et al.*, "A Tutorial on Environment-Aware Communications via Channel Knowledge Map for 6G," in *IEEE Communications Surveys & Tutorials*, vol. 26, no. 3, 2024.
Y. Zeng and X. Xu, "Toward Environment-Aware 6G Communications via Channel Knowledge Map," in *IEEE Wireless Communications*, vol. 28, no. 3, 2021.

Contact

Paul Berestesky: paul.berestesky@eit.lth.se

This project has received funding from the European Union's Horizon Europe research and innovation programme under the Marie Skłodowska-Curie grant agreement No 101119643, ultra-massive MIMO for future cell-free heterogeneous networks (MiFuture).

MiFuture
UMMIMO FOR 6G

MiFuture Newsletter

Robust High Mobility NLOS UE Beamforming Strategy for Gigantic MIMO

Josep R. Fernández Ruil
josep.fernandez@ericsson.com

ERICSSON
LUND UNIVERSITY

Abstract

Maintaining stable links in high-mobility scenarios is challenging for TDD-based gigantic MIMO systems, where rapid channel variations—especially under NLOS—quickly degrade reciprocity and beam alignment.

This work proposes a UE beamforming strategy that preserves link robustness without requiring extra pilot overhead by **aligning the UE's directional beam with its travel axis**. This movement-aligned beamforming minimizes the Doppler spread, directly increasing channel coherence. Simulations in scattering-rich cmWave environments confirm that travel-axis beamforming improves SNR stability, and reduces CSI-update demands, making it a promising technique for future high-mobility systems.

System Model

A scenario (Fig.1) with N_{UE} antennas at the UE, N_{BS} antennas at the BS, and N_{SC} scatterers is considered.

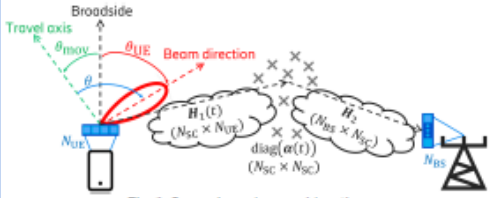

Fig. 1. Scenario under consideration

The receiver narrowband vector at the BS is:

$$y = H(t)w_{UE}s + n,$$

where s is the transmitted symbol assuming single-layer transmission, w_{UE} is the UE beamforming vector, $n \sim CN(0, N_0 I_{N_{BS}})$ is the noise vector, and $H(t)$ is the NLOS channel matrix given by

$$H(t) = H_2 \text{diag}(\alpha(t)) H_1(t),$$

where $H_1(t)$ is the time-varying channel matrix between the UE antennas and the scatterers, H_2 is the fixed channel matrix between the scatterers and the BS antennas, and $\alpha(t)$ is an N_{SC} sized vector containing the complex baseband respond of each of the N_{SC} scatterers.

BS Beamforming

$$w_{BS_{MRC}} = h_{est}^* / ||h_{est}||,$$

where $h_{est} = H(0)w_{UE}$, is estimated at $t = 0$. The resulting combiner maximizes the post-processing SNR at the BS.

UE beamforming

$$w_{UE} = \frac{1}{\sqrt{N_{UE}}} a_{UE}^*(\theta_{UE}),$$

being θ_{UE} the UE pointing direction

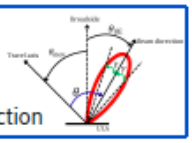

Travel-axis beamforming

$$\theta_{UE} \approx \theta_{mov}$$

The Doppler spread is minimized and makes the channel vary much more slowly over time, reducing how often beam updates are needed.

Results

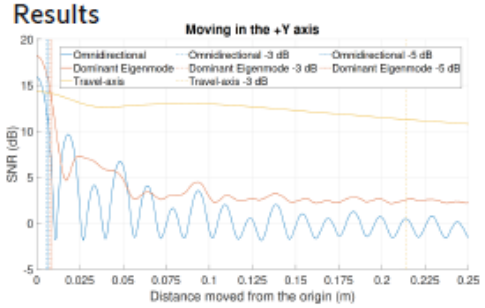

Fig. 2. SNR while the UE moves along the Y axis

The travel-axis strategy maintains a relevant more stable SNR level over a longer distance.

Conclusions

By aligning the beam with the UE trajectory, the temporal evolution of the channel is more stable, reducing the need for frequent channel updates while maintaining reliable communication performance.

This project has received funding from the European Union's Horizon Europe research and innovation programme under the Marie Skłodowska-Curie grant agreement No 101119643, ultra-massive MIMO for future cell-free heterogeneous networks (MiFuture).